

Soft Matter

Accepted Manuscript

This article can be cited before page numbers have been issued, to do this please use: M. Jyothi, M. Annadhasan, V. P. Vuppu and R. Chandrasekar, *Soft Matter*, 2020, DOI: 10.1039/D0SM00108B.



This is an Accepted Manuscript, which has been through the Royal Society of Chemistry peer review process and has been accepted for publication.

Accepted Manuscripts are published online shortly after acceptance, before technical editing, formatting and proof reading. Using this free service, authors can make their results available to the community, in citable form, before we publish the edited article. We will replace this Accepted Manuscript with the edited and formatted Advance Article as soon as it is available.

You can find more information about Accepted Manuscripts in the [Information for Authors](#).

Please note that technical editing may introduce minor changes to the text and/or graphics, which may alter content. The journal's standard [Terms & Conditions](#) and the [Ethical guidelines](#) still apply. In no event shall the Royal Society of Chemistry be held responsible for any errors or omissions in this Accepted Manuscript or any consequences arising from the use of any information it contains.

Journal Name

ARTICLE

Received 00th January 20xx,

Accepted 00th January 20xx

DOI: 10.1039/x0xx00000x

www.rsc.org/

Direct micro-scale monitoring of molecular aggregation, its growth and diffusion via aggregation-induced emission†

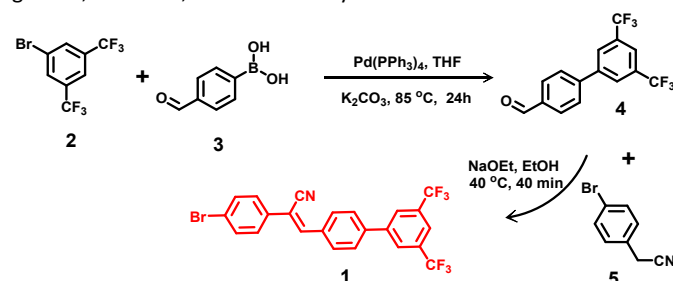
Mane Jyothi, Mari Annadhasan, Vinay Pradeep Vuppu, and Rajadurai Chandrasekar*

Time-dependent monitoring of aggregation-induced fluorescence of a model compound namely, (Z)-3-(3',5'-bis(trifluoromethyl)-[1,1'-biphenyl]-4-yl)-2-(4-bromophenyl)acrylonitrile unearths hitherto unknown molecular level events such as onset of molecular aggregation, their growth, size, and diffusion dynamics. The presented generalized approach can also be extended to in-situ monitoring and controlling of various biological aggregation processes down to a single-cell level and all aspects of materials chemistry, as well.

Molecular aggregation plays a pivotal role in many vital processes in nature and human-made materials. According to IUPAC definition, the term aggregation defines a “process whereby otherwise discrete molecules or particles form aggregates.”¹ Though aggregation is primarily an important process, the growth of aggregates in solution-phase is not well understood. At times, in dilute solutions, some π -molecular systems which are optically non-emissive reveal their emission at very high concentrations due to aggregation. The optical emission from the molecular aggregate arises because of the intramolecular conformation changes, which overpower the non-radiative pathway via the restriction of intramolecular rotations – known as aggregation-induced emission (AIE).^{2,3} The fluorescence (FL) spectroscopy snap-shots of AIE molecule aggregation process as a function of time could be extended to understand and regulate molecular or macromolecular level aggregation events in solution-phase. Investigation of molecular aggregation process is essential as it is unequivocally associated with (i) over human 50 diseases,⁴⁻⁷ including Alzheimer’s- and Parkinson’s-diseases and type II diabetes, and (ii) organic and polymer semiconductors device properties, such charge carrier mobility and electronic coupling^{8,9} and, so on. Importantly, apart from understanding different types of aggregate growth, it also essential to develop a technique that would allow

However, to our knowledge, concurrent investigation and control of the solution state dynamics of molecular-aggregation processes such as the formation of (detectable) microscale aggregates, their growth, concentration, and diffusion, are not studied in the literature. Hence, we envisioned exploiting an AIE-molecule to study the molecular-aggregation process. The investigations required time-correlated monitoring of the AIE intensity in dilute solution-, supersaturated solution- and solid-states during aggregation down to microsecond timescale with FL micro-spectroscopy.

For our studies we prepared a model AIE-molecule, namely, (Z)-3-(3',5'-bis(trifluoromethyl)-[1,1'-biphenyl]-4-yl)-2-(4-bromophenyl)acrylonitrile (**1**) shown in Scheme 1, which is structurally rather similar to 1-cyano-trans-1,2-bis-(3',5'-bis-trifluoromethyl-biphenyl) ethylene (CN-TFMBE).¹⁰ Both CN-TFMBE and **1** are structurally close as they possess a dominant electron-withdrawing cyano functionality anchored to the vinylene unit. In the solution state, due to bulky cyano-substitution, the CN-TFMBE experiences a non-planar conformation (twisted geometry and intramolecular rotation) and thereby annihilate the excitons non-radiatively rendering no or feeble emission.¹⁰ However, in the crystalline-state, the C-N...H hydrogen bonding interaction of the cyano group with phenyl hydrogens and π - π interactions limits the intramolecular rotation and provide rigidity, thus enhancing the optical emission.¹⁰⁻¹² As expected from the molecular structure, **1** emit cyan fluorescence (FL) via AIE mechanism. Here, we report the results on the time-correlated monitoring of polymorphic aggregate growth, their size, and diffusion dynamics.



Scheme 1 Synthetic scheme for the preparation of AIE molecule **1**.

School of Chemistry, University of Hyderabad
Prof. C. R. Rao Road, Gachibowli, Hyderabad-500046
India.

E-mail - r.chandrasekar@uohyd.ac.in

† Electronic Supplementary Information (ESI) available: [details of any supplementary information available should be included here]. See DOI: 10.1039/x0xx00000x

monitoring of the growth process.

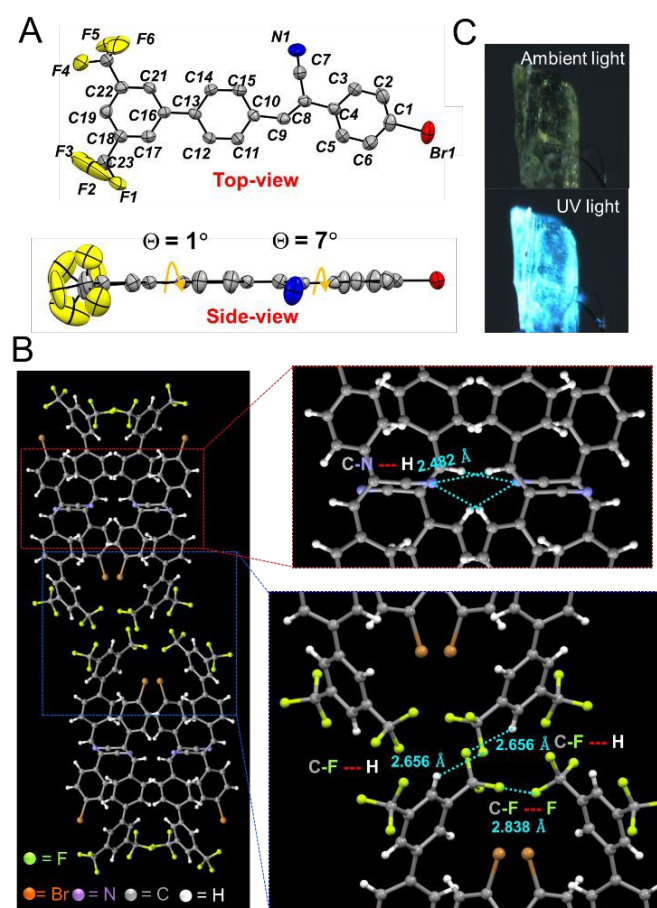


Fig. 1 A) ORTEP (50% probability thermal ellipsoids) views of **1**. All hydrogen atoms are omitted for clarity. B) Solid-state molecular packing of **1**. C) Photographs of crystal **1** under ambient and UV light, respectively.

The synthesis of **1** required precursor compounds **4** and **5**. At first, compound **4** was prepared via Suzuki cross-coupling by reacting 1-bromo-3,5-bis(trifluoromethyl)benzene **2** with the 4-formyl phenyl boronic acid **3** in 89% yield. Condensation of **4** and 2-(4-bromophenyl)acetonitrile **5** provided target AIE molecule **1** with 94% (Scheme 1). Crystallization of molecule **1** in chloroform produced needle-shaped crystals with a square-shaped cross-wise geometry. The X-ray analysis [CCDC: 1971747] of single crystal revealed a near planar conformation of **1** (Figure 1A). The torsion angles between bromophenyl and the vinyl units and trifluoromethyl substituted biphenyl units were 7° and 1° , respectively. Molecule **1** possesses intermolecular C-F...H (2.656 Å) and C-N...H (2.482 Å) H-bonding interactions and also π - π interactions (3.713 Å) (Figure 1B and Fig. S9).

In the solution-state, compound **1** showed subtle luminescence upon excitation with UV light (365 nm). The emission spectrum exhibited peaks around 370, 411 and 433 nm with a meagre quantum yield of 1.38% (see Figure S3). The steady-state FL spectra of **1** in acetonitrile showed increased AIE intensity upon addition of (poor solvent) water or viscous solvents (Figure S6 and S8). Self-assembly of compound **1** in acetonitrile or chloroform formed rod-

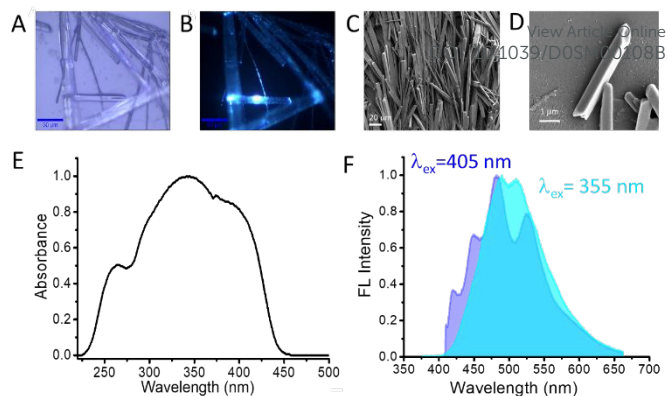


Fig. 2 A and B) Optical and FL microscopy images of microcrystals of **1**, respectively. C and D) FESEM images of microcrystals of **1**, E) Solid-state absorbance and F) FL spectra of **1** with two different laser excitations (355 and 405 nm), respectively.

shaped active optical waveguiding¹³ bright cyan emitting microcrystals (Figure 2A,B and Figure S5). Field emission scanning microscope (FESEM) images revealed the square-shaped cross-section of the one-dimensional micro-crystals (Figure 2C, D and S4). Micro-crystals of **1** showed an extended absorption band up to 450 nm (Figure 2E). Optical excitation of micro-crystals with a 355 nm laser displayed FL spectra with two distinctive bands with multiple shoulders (Figure 2F). However, excitation of the same micro-crystals with 405 nm laser resolved the spectral features very well and revealed the shoulder peak positions at 420, 447, 477 and 523 nm (Figure 2F). This laser-light-dependent spectral transformation also indicates the sensitivity of the molecular crystals for different polarization directions of the laser source. The origin of greenish-blue (cyan) colour is due to the appearance of intense peaks at 477, 479 and 525 nm with the spectral tail extended up to 675 nm (Figure 1C). The cyan AIE originate as a result of restricted intramolecular rotations and near planar conformation, both enable an efficient π -conjugation providing AIE for compound **1**.¹⁴ The solid-state absolute FL quantum yield of the aggregate **1** is 11%.

Generally, the morphology of evolving molecular aggregate during self-assembly is concentration-dependent, which fluctuates due to random flow of evaporating solvent. Therefore, the dynamics of the molecular aggregation process was probed *in-situ* with confocal FL micro-spectroscopy (camera speed at 25 fps) shown in the inset of Fig. 3A. The sample was excited using a 405 nm laser (reflection mode; objective 20 \times ; numerical aperture = 0.4). Initially, by placing an acetonitrile solution of **1** ($c = 2$ mM; volume = 50 μ L) on a coverslip the onset of AIE intensity during solvent evaporation (within 200 s) was collected from multiple areas. For every 0.3 s the AIE (if any) was collected by a CCD detector for the duration of up to 0-300 s. Each experiment (see Figure 3A) revealed random time-dependent AIE signal counts (from several thousand to ~ 3 million). Significantly, the dynamic AIE counts provide a qualitative estimate of the time-dependent (fluctuating) aggregate(s) size (concentration) in a given micro-volume during solvent evaporation.

To comprehend the reason behind time-dependent fluctuating AIE counts, six peculiar-looking plots (*viz.*, I to IX) were identified for scrutiny (Figure 3 B-J). Plot-I, presented in Figure 3B showed no AIE

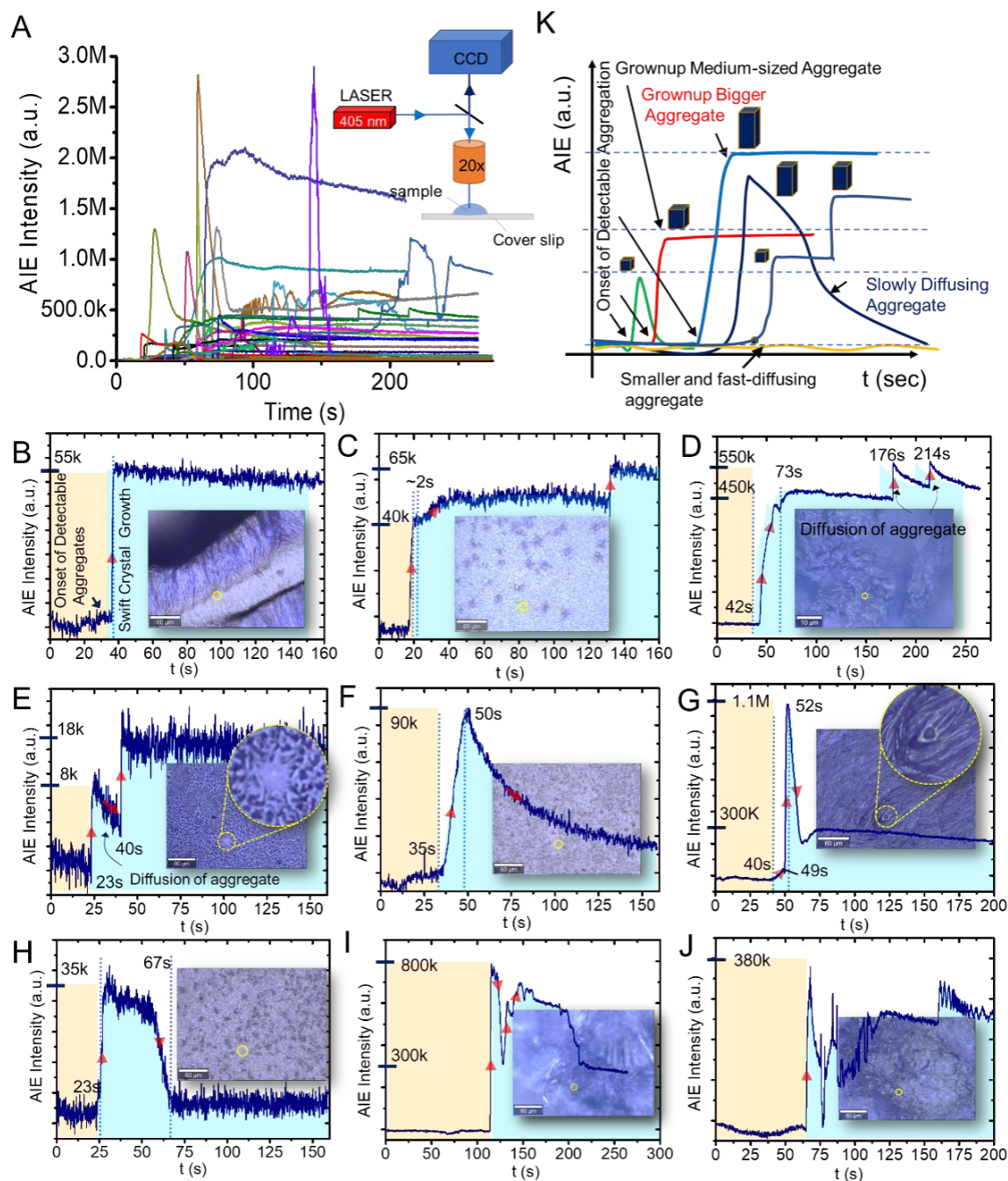


Fig. 3 A) Time-dependent AIE intensities of hundreds of experiments. The inset shows the cartoon of the FL-micro-spectrometer. B-J) AIE intensity versus time plots of six representative experiments. The insets show the confocal optical images taken immediately after the experiment. The yellow circles of the insets show the laser excitation area. K) Pictorial representation of the various process involved during the aggregate growth.

signal until 40 s, indicating no recordable molecular aggregation. Beyond 40 s, the AIE signal quickly appeared, and its intensity increased swiftly (vertically) to about 55 k counts within 1 s. The

sharp rise of AIE intensity signifies the onset of the spectroscopically observable aggregate growing to reach a specific size. Afterwards, the AIE counts persisted till complete solvent

vaporisation indicating cessation of the aggregate growth. The micro-area image revealed the fibrous morphology of the grown aggregates (see Figure 3B inset). The course of AIE counts as a function of time in Plot-II (Figure 3C) was slightly different from Plot-I. In the beginning, a typical fast-growth (within 2 s) from the onset of detectable aggregate occurred with AIE counts reaching 40k at 20 s; subsequently, after initial slow growth, the aggregate size remained constant till 132 s. Surprisingly, over again, the AIE intensity vertically soared to 55 k at 133 s specifying further growth of the aggregate or sudden diffusion of another aggregate towards the growing aggregate.

In Plot-III (Figure 3D), the AIE counts revealed that the growth of visible aggregate started after 42 s. Later, after a nearly 31 s the AIE counts reached a transiently stable state with 450 k, and was stable till 176 s. The growth track of the aggregate involved three steps; initially steep progress, then sluggish, and later a slight back-and-forth diffusion (see v-shaped dip) from the growth site. The shape of the curve and the AIE counts reveal the slow growth rate and larger size of the aggregate, respectively, compared to the previous two cases. After 125 s, surprisingly, two peaks appeared at 176 and 214 s with a sudden surge of the AIE intensity up to 550 k. The rise and fall (about 100 k) of AIE intensity twice imply jiggle movements of the smaller aggregate towards the bigger one. The path of the curve between the two peaks (time gap: 86 s) indicates an abrupt (<1 s) diffusion of a smaller aggregate towards (with a 100 k AIE count) the bigger one, followed by its gentle diffusion away (~86 s) from it.

Interestingly, the curve displayed in Figure 3E (Plot-IV) exhibited two steep growth steps with AIE counts reaching 8 and 18 k, respectively. In between the two vertical growth lines, a slight decline of counts point towards slow diffusion (~17 s) of a fast-growing aggregate from the observation area. Beyond 40 s, the aggregate stabilised its position without any substantial growth and diffusion. Here, the meagre counts and the signal-to-noise ratio hint towards a much smaller size of the aggregate. Additionally, the optical image recorded immediately after the experiment (inset of Figure 3E) and the video revealed a cluster of small fibres excluding the area irradiated with the laser beam indicating diffusion of fibres away from the light beam during their growth. Remarkably, the shape of the curve shown as Plot-V in Figure 3F revealed a less complicated path taken by the particular aggregate. Here, the aggregate slowly and steadily grew for nearly 15 s and then gradually diffused away from the observation area in 2 min.

On the contrary, in Plot-VI, after 40 s, with an initial lag of 9 s, the aggregate grew much bigger quickly reaching a colossal AIE count of 1.1 M in 3 s and later, it diffused away rather fast but not entirely from the observation area (Figure 3G). The inset image of Fig. 4G, captured immediately after the experiment showed aligned fibres and also revealed a local disturbance in the fibre organisation around the laser illumination area (see the yellow circle). In case-VII presented in Figure 3H, the shape of the curve (with two slope values) between 23 s and 67 s indicates that after rapid growth, the aggregate diffusion is initially slow and later quick. An intricate pattern of the curves shown in Figure 3I and J (Plot-VIII and -IX)

imply complex (multiple) diffusion dynamics of the micro-crystal(s) after its(their) growth in the evaporating solvent medium.

In conclusion, we demonstrated a robust technique to follow the molecular aggregates process using confocal micro-FL spectroscopy. From the time-correlated monitoring of AIE intensity, the following key characteristics of molecular aggregates (Figure 3K) can be inferred.

- A range of detectable aggregation time indicates a varying growth rate of molecular aggregate in different areas of the sample.
- The variation of the AIE intensity correlates directly with the size and concentration of the aggregates in a given area. Higher AIE counts revealed the existence of bigger-sized and tightly-packed aggregates in contrary to smaller-sized and dispersed aggregate with lower AIE counts.
- The decrease of the AIE intensity at varying rates indicates diffusion of the aggregates caught in the solvent convection current.
- The diffusion dynamics of bigger-sized aggregate in the crowded regions are more prominent than the smaller-sized ones.
- The horizontal lines or a constant AIE intensity point to stable aggregate(s) without growth and diffusion.

Our original findings provide new insights and illustrate practical experimental protocols which can be applied to (i) probe the concentration change in a specific site down to the single-cell level, and (ii) monitor aggregation dynamics and motion of biomacromolecules tagged with AIE luminogens.

Conflicts of interest

There are no conflicts to declare.

Acknowledgements

This work was financially supported by DST (New Delhi; Grant No. INT/RUS/RSF/P-05) and SERB (CRG-2018/001551). M. J. and V. V. P. thank CSIR for JRFs.

References

- 1 J. Alemán, A. V. Chadwick, J. He, M. Hess, K. Horie, R. G. Jones, P. Kratochvil, I. Meisel, I. Mita, G. Moad, S. Penczek and R. F. T. Stepto, *Pure Appl. Chem.*, 2007, **79**, 1801-1829.
- 2 J. Luo, Z. Xie, J. W. Y. Lam, L. Cheng, H. Chen, C. Qiu, H. S. Kwok, X. Zhan, Y. Liu, D. Zhu and B. Z. Tang, *Chem. Commun.*, 2001, 1740-1741.
- 3 J. Shi, L. E. A. Suarez, S.-J. Yoon, S. Varghese, C. Serpa, S. Y. Park, L. Lüer, D. Roca-Sanjuán, B. Milián-Medina and J. Gierschner, *J. Phys. Chem. C.*, 2017, **121**, 23166-23183.
- 4 C. M. Dobson, *Nature*, 2003, **426**, 884-890.
- 5 J. Hardy, and D. J. Selkoe, *Science* 2002, **297**, 353-356.
- 6 S. L. Bernstein, N. F. Dupuis, N. D. Lazo, T. Wyttenbach, M. M. Condron, G. Bitan, D. B. Teplow, J. -E. Shea, B. T. Ruotolo, C. V. Robinson and M. T. Bowers, *Nat. Chem.*, 2009, **1**, 326-331.

Journal Name

ARTICLE

- 7 R. Kayed, E. Head, J. L. Thompson, T. M. McIntire, S. C. Milton, C. W. Cotman and C. G. Glabel, *Science*, 2003, **300**, 486-489.
- 8 T. Eder, T. Stang, M. Gmelch, K. Remmerssen, D. Laux, S. Hoyer, J. M. Lupton, and J. Vogelsang, *Nat. Commun.* 2017, **8**:1641.
- 9 S. Wang, S. Fabiano, S. Himmelberger, S. Puzinas, X. Crispin and M. Berggren, *Proc. Natl. Acad. Sci. USA*, 2015, **112**, 10599-10604.
- 10 J. W. Chung, B. K-. An and S. Y. A. Park, *Chem. Mater.*, 2008, **20**, 6750-6755.
- 11 J. Mei, N. L. C. Leung, R. T. K. Kwok, J. W. Y. Lam, and B. Z. Tang, *Chem. Rev.* 2015, **115**, 11718–11940.
- 12 H. Wang, E. Zhao, J.W.Y. Lam, B. Z. Tang, *Mater. Today*, 2015, **18**, 365-377.
- 13 N. Chandrasekhar, S. Basak, and M. A. Mohiddon, R. Chandrasekar, *ACS Appl. Mater. Inter.* 2014, **6**, 1488-1494.
- 14 Y. H. Jacky, W. Y. Lam and B. Z. Tang, *Chem. Soc. Rev.*, 2011, **40**, 5361-5388.

View Article Online
DOI: 10.1039/D0SM00108B